11C Radiolabeling of anle253b: a Putative PET Tracer for Parkinson's Disease That Binds to α-Synuclein Fibrils in vitro and Crosses the Blood-Brain Barrier

Andreas Maurer,*[a] Andrei Leonov,[b, d] Sergey Ryazanov,[b] Kristina Herfert,[a] Laura Kuebler,[a] Sabrina Buss,[a] Felix Schmidt,[c] Daniel Weckbecker,[c] Ruth Linder,[b] Dirk Bender,[e] Armin Giese,[c, d] Bernd J. Pichler,[a] and Christian Griesinger*[b, d]

There is an urgent clinical need for imaging of α-synuclein (αSyn) fibrils, the hallmark biomarker for Parkinson's disease, in neurodegenerative disorders. Despite immense efforts, promising tracer candidates for nuclear imaging of αSyn are rare. Diphenyl pyrazoles are known modulators of αSyn aggregation and thus bear potential for non-invasive detection of this biomarker in vivo. Here we demonstrate high-affinity binding of the family member anle253b to fibrillar αSyn and present a high-yielding site-selective radiosynthesis route for 11C radiolabeling using in-situ generated [11C]formaldehyde and reductive methylation. Radio-HPLC of the tracer after incubation with rat serum in vitro shows excellent stability of the molecule. Positron emission tomography in healthy animals is used to assess the pharmacokinetics and biodistribution of the tracer, showing good penetration of the blood–brain barrier and low background binding to the non-pathological brain.

[a] Dr. A. Maurer, Dr. K. Herfert, L. Kuebler, S. Buss, Prof. Dr. B. J. Pichler
Werner Siemens Imaging Center, Department of Preclinical Imaging and Radiopharmacy
Eberhard Karls University Tübingen
Röntgenweg 15
72076 Tübingen (Germany)
E-mail: andreas.maurer@med.uni-tuebingen.de

[b] Dr. A. Leonov, Dr. S. Ryazanov, R. Linder, Prof. Dr. C. Griesinger
Department of NMR-based Structural Biology
Max Planck Institute for Biophysical Chemistry
Am Fassberg 11
37077 Göttingen (Germany)
E-mail: cigr@nmr.mpibpc.mpg.de

[c] Dr. F. Schmidt, Dr. D. Weckbecker, Prof. Dr. A. Giese
Center for Neuropathology and Prion Research
Ludwig Maximilians University
Feodor-Lynen-Str. 23
81377 Munich (Germany)

[d] Dr. A. Leonov, Prof. Dr. A. Giese, Prof. Dr. C. Griesinger
MODAG GmbH
Mikro-Forum-Ring 3
55234 Wendelsheim (Germany)

[e] Prof. Dr. D. Bender
Department for Nuclear Medicine and PET Center
Aarhus University Hospital
Palle Juul-Jensens Boulevard 165
8200 Aarhus (Denmark)

Due to setbacks with clinical trials in neurodegenerative diseases, early disease detection and monitoring of disease-modifying therapies are becoming increasingly important. Groundbreaking work enabled nuclear (positron emission tomography, PET) imaging and longitudinal quantification of β-amyloid (Aβ) plaques in Alzheimer's disease, now routinely used in clinical research.[1] This greatly contributed to advanced understanding of the pathogenesis and development of the disease.[2] In contrast, despite great public attention and large-scale initiatives, no clinically evaluated radiotracers are currently available to detect aggregation of α-synuclein (αSyn) to Lewy Bodies,[3] the pathological hallmark of Parkinson's disease, dementia with Lewy Bodies, multiple systems atrophy and other, less frequent neurodegenerative diseases.[4] Not only precise diagnosis of these diseases but also deeper understanding of the interplay between αSyn aggregation and progressive neurodegeneration[5] and the crosstalk between the different αSyn, Aβ and tau pathologies[6] would benefit from sensitive real-time detection and quantification of αSyn in patients. Most importantly, αSyn imaging would be a major pillar besides the clinical disease rating scales for evaluation of therapeutic approaches.

This unmet demand for αSyn radiotracers comes up against the only few known groups of small-molecule compounds interacting with aggregated αSyn with notable affinity and selectivity, mainly phenothiazines,[7] other fluorescent dyes[8] and compounds based on 3-(benzylidene)indolin-2-one.[9] Diphenylpyrazoles such as anle138b (**1**) were identified from a large-scale screening to inhibit pathological aggregation of prion protein (PrPsc) and αSyn in vivo[10] and their direct binding to αSyn fibrils was demonstrated in vitro by fluorescence spectroscopy.[11] This led us to the hypothesis that the anle138b family might represent good candidates for the development of PET tracers for αSyn aggregation. As anle253b (**2**) from the compound list originally reported[12] bears a methyl group suitable for 11C-methylation ($t_{1/2} = 20.3$ min) we selected this compound as a starting point for tracer development. Previous reports demonstrated αSyn aggregation inhibition of 50% in the reported *scanning for intensely fluorescent targets* assay[13] and a brain uptake in mice of 2.1 nmol/g four hours after oral application of 1 mg (ca. 40 mg/kg).

The most common approach for 11C radiolabeling is methylation by means of [11C]methyl iodide (MeI) or [11C]methyl

triflate (MeOTf). These methylating agents can be efficiently synthesized from cyclotron-produced [^{11}C]CO$_2$ using automated gas-phase reactions on commercially available synthesizers. The alternative synthon [^{11}C]formaldehyde (CH$_2$O) is less commonly applied since its preparation required the more complicated "wet method" and thus specialized radiochemistry modules. Groundbreaking work from Hooker et al.[14] has enabled the synthesis of [^{11}C]CH$_2$O from [^{11}C]MeI by oxidation with trimethyl-N-oxide (TMAO), making radiosynthesis with [^{11}C]CH$_2$O an easily available and attractive alternative to the classical methylating reagents. Reductive radiomethylation using [^{11}C]CH$_2$O was successfully applied to primary aromatic amines. Among others, the Pittsburgh compound B, a PET tracer used in studies of Alzheimer's disease, was prepared using this method.[15]

In this work, we describe the radiosynthesis of [^{11}C]2 from its desmethyl precursor 3 exploiting the distinct site-selectivity of [^{11}C]CH$_2$O and [^{11}C]MeI. We show data for specific binding of [^{11}C]2 to αSyn fibrils in vitro and analyze the time-dependent biodistribution of the tracer in vivo using PET imaging.

First, we characterized the fibril binding of 2 using a competition assay with tritiated 1 on recombinant human αSyn fibrils. This assay showed high-affinity binding of 2 to αSyn fibrils with an IC$_{50}$ value of 1.6 nM, making this compound a promising candidate for imaging synucleinopathies (Figure 1).

We then set out to directly methylate 3 with [^{11}C]MeI. We expected the reaction to concurrently occur both at the aniline nitrogen and the pyrazole nitrogen atoms, with a tendency for aniline methylations with weaker bases or with no additional base added. Indeed, when we performed radiomethylation reactions with Cs$_2$CO$_3$ addition (Table 1, line 2), we found that the radioactivity was nearly quantitatively incorporated as pyrazole-methylated [^{11}C]4 and 5 (in a ratio of about 5:2, respectively), while only minor radioactivity peaks were

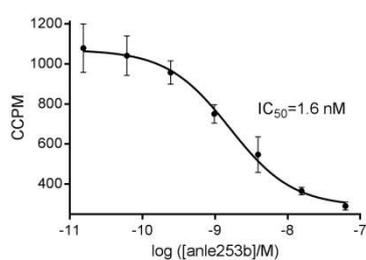detected at the retention time of 2 (Figure 2A and Table 1) under the various conditions applied. By omitting additional base we were able to completely suppress pyrazole methylations but still only achieved low radiochemical conversions of <15%. While further optimization might be possible using longer beam-times, higher temperatures, or MeOTf as methylating agent, we hypothesized that reductive methylation with formaldehyde might be a more efficient route for radiosynthesis of [^{11}C]2 due to the expected selectivity for primary amines.

Screening of suitable reducing agents (Suppl. Scheme 3) led to the identification of sodium cyanoborohydride and a mixture of phosphate buffer and dimethylformamide (DMF) as the best combination for this reaction. According to literature evidence[15] suggesting dimethylformamide as a possible reason of specific activity erosion, diethylformamide (DEF) was selected as solvent. Fine tuning of buffer pH led to a slightly increased yield of target product 2 at a pH of 5.

When we applied these conditions to radiolabeling, we immediately observed formation of the desired product in reasonable yields (>300 MBq), without generation of the previously observed side products. This indicates that canonical and reductive radiomethylation can be used as orthogonal strategies for radiolabeling of the aniline-containing branch of the anle138b (1) family (Scheme 1), enabling selective production of three different radiotracers from a single precursor.

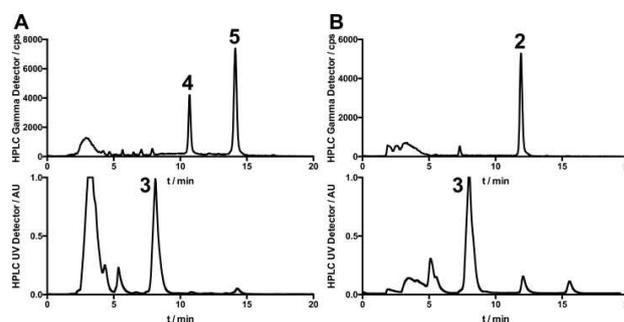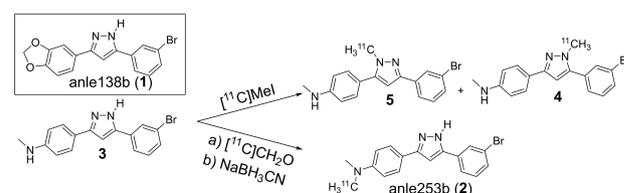**Figure 1.** Competitive binding of 2 and [^{3}H]1 to αSyn fibrils. Fibrils were probed with tritiated 1 (1 nM) in the presence of a dilution series of 2. Mean values ±SD (n=3) are presented.

Figure 2. Exemplary results from substitutive (A) and reductive (B) radiomethylation of 3. A: [^{11}C]MeI was trapped in a solution of 1 mg 3 and 5 mg Cs$_2$CO$_3$ in 500 µl DMSO and heated to 110 °C for 5 min. [^{11}C]4 and 5 are the main products while no [^{11}C]2 is formed. B: [^{11}C]MeI was trapped in a solution of 5 mg TMAO and 1 mg 3 in 350 µl DEF cooled to −20 °C. After incubation at 60 °C for 3 min, 7.6 mg NaBH$_3$CN in 60 µl DEF and 1.2 mL 100 mM citrate phosphate buffer pH 5 were added and the resulting mixture was heated to 100 °C for 5 min. [^{11}C]2 was the main radioactive product. The precursor 3 is visible in both UV chromatograms.

Table 1. Conditions for direct radiomethylation of 3 with MeI. Reaction time for all reactions was set to 5 min. Radiochemical conversions (%) were calculated from semipreparative HPLC chromatograms.

Solvent	Base	Temperature [°C]	2 [%]	4 [%]	5 [%]
DMSO	NaOH, 5 µL 5 M	110	0	28.2	58.5
DMSO	Cs$_2$CO$_3$	110	0	18.4	45.4
DMSO	NaHCO$_3$	110	2.1	7.2	14.6
DMSO	–	110	9.3	0	0
DMF	–	110	0	0	0

Scheme 1. Structure of anle138b (1), and reaction scheme for ^{11}C-radiomethylation of 3 using either nucleophilic substitution or reductive methylation selectively yielding pyrazole-methylated 4 and 5 or aniline-methylated 2, respectively.

Figure 2B shows a typical chromatogram from such an experiment. After some experiments with separate additions of **3** and the reducing agent after the TMAO reaction we found that **3** can already be added to the TMAO solution without negatively affecting the outcome of the reaction. Omitting TMAO from this solution massively reduced the formation of **2** from 47% to only 5% (radiochemical conversion), demonstrating that the reaction is indeed mainly mediated by TMAO-dependent formaldehyde formation. Using this synthesis route we reliably obtained yields of 600–2000 MBq [^{11}C]**2** after 30 min (35 µAh) target irradiation. Although this methylation approach enabled high radiochemical yields, the obtained molar radioactivities were comparatively low (15.1 ± 3.4 GBq/µmol at end of synthesis. For other tracers we typically achieve 60–200 GBq/µmol) and the synthesis thus requires further optimization for successful imaging of low-abundant targets such as αSyn aggregates. Regardless of this remaining challenge, the reliable and high-yielding radiosynthesis approach allowed us to analyze the in vitro and in vivo characteristics of **2**.

To assess serum stability of [^{11}C]**2**, rat serum was incubated with the tracer at 37 °C for 1.5 hours and analyzed by radio-HPLC. The chromatograms (Suppl. Fig. 2) did not show any signs of metabolism or degradation of [^{11}C]**2** in serum over 90 minutes.

After immobilizing αSyn in microtiter plates and probing it with [^{11}C]**2** we quantified the bound activity using autoradiography. We were able to detect statistically significant ($p = 0.0167$, Tukey's test) fibril binding of the tracer that was blockable ($p = 0.0057$, Tukey's test) to baseline levels by excess (1 µM) of the non-radioactive compound (Figure 3A). When we
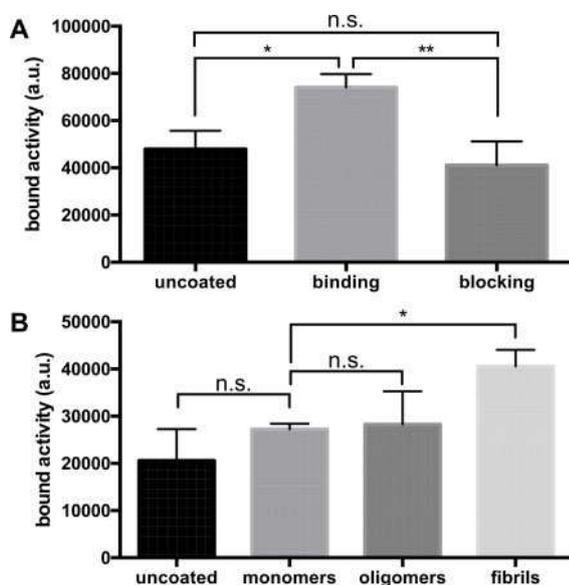
coated the plate with different oligomerization states, [^{11}C]**2** showed preferential binding to αSyn fibrils (Figure 3B) compared to oligomers (not significant, Dunnett's test) and monomers ($p = 0.0341$, Dunnett's test). The low signal intensity in this assay only allowed for qualitative verification of [^{11}C]**2** fibril binding within the scope of this work, while quantification of binding data (in addition to abovementioned IC$_{50}$) will be established in future using our tritium-based assay.

When designing PET tracers for brain imaging, not only affinity and selectivity but also suitable physicochemical properties like the log$P$ value and molecular weight are crucial constraints. Log$P$ values between 1 and 4 are considered as optimal, depending on the author,[16] although the meaningfulness of log$P$ is under discussion.[17] With its (calculated) log$P$ of 5.21, **2** is not considered optimal in this regard and might show a tendency for unspecific lipid binding but seemed lipophilic enough to cross the blood–brain barrier. We thus analyzed the in vivo biodistribution after tail vein injection in healthy rats. During the dynamic PET scans the tracer [^{11}C]**2** showed a clear penetration of the blood brain barrier in all animals. It is homogenously distributed in the complete brain with a higher midbrain uptake (Figure 4A). This is also observed in the kinetics of the tracer where the lowest uptake of [^{11}C]**2** is seen in the cortex. Figure 4B shows the uptake kinetics (%ID/cm^3) for the cerebellum, brainstem, cortex and striatum with an initial perfusion peak after the injection. After a drop, a slow increase can be observed until 25 minutes after injection, followed by a slow washout of the activity.

Ex vivo biodistribution was carried out directly after PET measurements with [^{11}C]**2**. The data are presented in Figure 4C. The highest activity concentrations (in %ID/g) are observed in the left and right kidney (0.52 ± 0.30, 0.69 ± 0.17 respectively) as well as in the liver (0.79 ± 0.22) which might represent excretion of the tracer after 75 minutes of PET measurement. In the brain, the cortex and the cerebellum show the lowest radioactivity concentration (0.25 ± 0.05, 0.24 ± 0.05 %ID/g) whereas the brainstem shows the highest uptake values (0.30 ± 0.05 %ID/g).

In vivo stability was analyzed by injection of the radiotracer into healthy rats (178.5 ± 35.8 MBq) and HPLC analysis of cleared brain lysates and plasma samples after 7 and 15 minutes (see Suppl. Figure 5). Despite the low sensitivity of our radio-HPLC detector we were able to verify that the majority of radioactivity in the brain was indeed [^{11}C]**2** at 7 min and 15 min post injection.

The overall distribution and in particular the pattern within the brain seems to be suited for application in relevant animal models, although the time-activity curves showed atypical brain uptake kinetics after the typical drop following the perfusion peak. This might be caused by the rather high log$P$ value and will require deeper kinetic analysis using a blood sampling approach to record the arterial input function. To exclude suboptimal serum stability of the tracer as an alternative explanation of the unexpected time-activity curve, we analyzed the stability of [^{11}C]**2** by co-incubation with rat serum. Since the tracer was completely stable within the time of incubation, metabolism (e.g. cytochrome P450-mediated demethylation) in a different organ with efficient release of metabolites back into
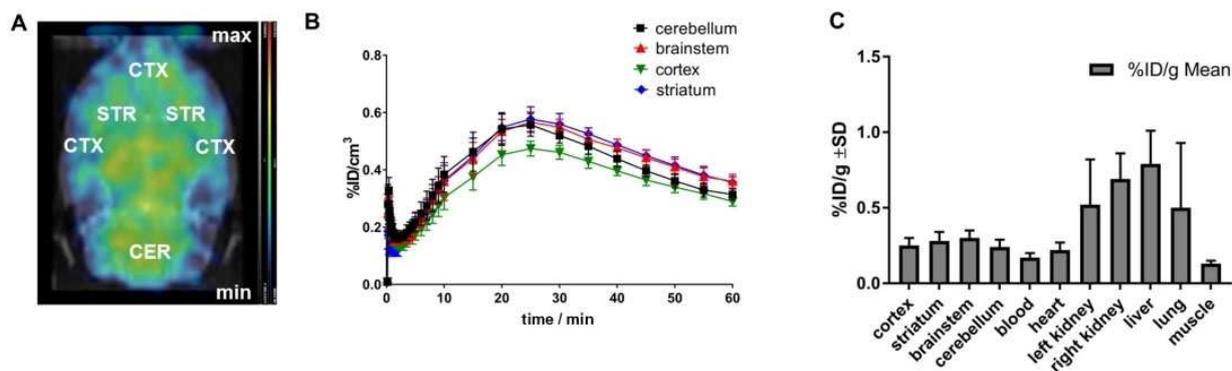

Figure 3. Binding assays using αSyn fibrils. A: αSyn fibrils were incubated with 3 nM [^{11}C]**2** in the presence (blocking) or absence (binding) of 1 µM of the non-radioactive compound. Wells containing no αSyn fibrils ("uncoated") were used as negative control. Binding to αSyn fibrils was statistically significant ($p = 0.0167$) and completely blocked ($p = 0.0057$) by addition of excess **2**. B: Three different states of αSyn were used for coating of the plate. [^{11}C]**2** preferentially bound to fibrillar synuclein ($p = 0.0341$). Binding was not statistically significant (n.s.) for monomeric and oligomeric αSyn.

Figure 4. Pharmacokinetic characteristics of [^{11}C]**2** in healthy rats ($n = 4$, mean values $\pm$ SD). A: Dynamic PET scan (coronal plane) of all 39 frames of the brain demonstrates brain uptake and distribution suited for imaging with even distribution of [^{11}C]**2** in the whole brain. B: Brain uptake of [^{11}C]**2** drops after the initial perfusion peak and then slowly increases over time to a maximum uptake after 25 min, after which the activity slowly washes out. C: Ex vivo biodistribution after 75 min uptake time shows median uptake values in the brain between 0.24 ± 0.05 (cerebellum) and 0.30 ± 0.05 %ID/g (brainstem). Organ uptake was highest in the liver with 0.79 ± 0.22 %ID/g.

the serum and accumulation of the metabolite might cause atypical brain uptake. This, however, was not supported by ex vivo HPLC of brain lysates where the main radioactivity 15 min post injection was found in the form of the parent compound.

To use the brain time-activity curves for calculation of binding potential maps, we are now applying more sophisticated approaches involving the arterial input function, and in parallel we are following up on potential tissue metabolism. This will allow us to further improve the tracer regarding both pharmacokinetics and metabolic stability, as well as quantification of αSyn in disease models, going beyond this study in healthy animals where we would not expect αSyn binding.

Taken together, we utilize the reductive methylation approach for site-selective radiosynthesis of [^{11}C]**2** and demonstrate synuclein fibril binding in vitro and blood brain barrier penetration in healthy rats in vivo. This is the first report of ^{11}C radiosynthesis and biodistribution analysis of this compound class. Next steps will focus on improvement of the clog*P* value, optimization of uptake dynamics and quantification of selectivity between αSyn and other types of aggregates. Improved next-generation candidates will be evaluated in animal models of disease and on human pathological tissues. Although further work is needed, these compounds might bear the potential for longitudinal quantification of αSyn aggregates both in animal models, and in patients suffering from synucleinopathies.

Experimental section

Experimental details are found in the Supporting Information.

Acknowledgements

[1] W. E. Klunk, H. Engler, A. Nordberg, Y. M. Wang, G. Blomqvist, D. P. Holt, M. Bergstrom, I. Savitcheva, G. F. Huang, S. Estrada, B. Ausen, M. L. Debnath, J. Barletta, J. C. Price, J. Sandell, B. J. Lopresti, A. Wall, P. Koivisto, G. Antoni, C. A. Mathis, B. Langstrom, *Ann. Neurol.* **2004**, *55*, 306–319.

[2] R. L. Buckner, A. Z. Snyder, B. J. Shannon, G. LaRossa, R. Sachs, A. F. Fotenos, Y. I. Sheline, W. E. Klunk, C. A. Mathis, J. C. Morris, M. A. Mintun, *J. Neurosci.* **2005**, *25*, 7709–7717.

[3] J. L. Eberling, K. D. Dave, M. A. Frasier, *J Parkinson Dis* **2013**, *3*, 565–567.

[4] H. McCann, C. H. Stevens, H. Cartwright, G. M. Halliday, *Parkinsonism Relat Disord* **2014**, *20 Suppl 1*, S62–67.

[5] T. E. Golde, *Mol. Neurodegener.* **2009**, *4*.

[6] P. T. Kotzbauer, N. J. Cairns, M. C. Campbell, A. W. Willis, B. A. Racette, S. D. Tabbal, J. S. Perlmutter, *Arch Neurol-Chicago* **2012**, *69*, 1326–1331.

[7] L. H. Yu, J. Q. Cui, P. K. Padakanti, L. Engel, D. P. Bagchi, P. T. Kotzbauer, Z. D. Tu, *Bioorgan Med Chem* **2012**, *20*, 4625–4634.

[8] K. L. Neal, N. B. Shakerdge, S. S. Hou, W. E. Klunk, C. A. Mathis, E. E. Nesterov, T. M. Swager, P. J. McLean, B. J. Bacskai, *Mol. Imaging Biol.* **2013**, *15*, 585–595.

[9] W. H. Chu, W. Zhou, V. Gaba, J. L. Liu, S. H. Li, X. Peng, J. B. Xu, D. Dhavale, D. P. Bagchi, A. d'Avignon, N. B. Shakerdge, B. J. Bacskai, Z. D. Tu, P. T. Kotzbauer, R. H. Mach, *J. Med. Chem.* **2015**, *58*, 6002–6017.

[10] a) J. Levin, J. Wagner, S. Ryazanov, A. Leonov, S. Shi, F. Schmidt, C. Prix, U. Bertsch, G. Mitteregger-Kretzschmar, M. Geissen, T. Hirschberger, P. Tavan, J. Pilger, M. Zweckstetter, T. Frank, M. Baehr, J. Weishaupt, M. Uhr, H. Urlaub, U. Teichmann, K. Boetzel, M. Groschup, H. A. Kretzschmar, C. Griesinger, A. Giese, *Movement Disord* **2011**, *26*, S21-S21; b) A. Heras-Garvin, D. Weckbecker, S. Ryazanov, A. Leonov, C. Griesinger, A. Giese, G. K. Wenning, N. Stefanova, *Mov Disord* **2019**, *34*, 255–263.

[11] A. A. Deeg, A. M. Reiner, F. Schmidt, F. Schueder, S. Ryazanov, V. C. Ruf, K. Giller, S. Becker, A. Leonov, C. Griesinger, A. Giese, W. Zinth, *Bba-Gen Subjects* **2015**, *1850*, 1884–1890.

[12] J. Wagner, S. Ryazanov, A. Leonov, J. Levin, S. Shi, F. Schmidt, C. Prix, F. Pan-Montojo, U. Bertsch, G. Mitteregger-Kretzschmar, M. Geissen, M. Eiden, F. Leidel, T. Hirschberger, A. A. Deeg, J. J. Krauth, W. Zinth, P. Tavan, J. Pilger, M. Zweckstetter, T. Frank, M. Bahr, J. H. Weishaupt, M. Uhr, H. Urlaub, U. Teichmann, M. Samwer, K. Botzel, M. Groschup, H. Kretzschmar, C. Griesinger, A. Giese, *Acta Neuropathol.* **2013**, *125*, 795–813.

[13] U. Bertsch, K. F. Winklhofer, T. Hirschberger, J. Bieschke, P. Weber, F. U. Hartl, P. Tavan, M. Tatzelt, H. A. Kretzschmar, A. Giese, *J. Virol.* **2005**, *79*, 7785–7791.

[14] J. M. Hooker, M. Schoenberger, H. Schieferstein, J. S. Fowler, *Angew. Chem. Int. Ed.* **2008**, *47*, 5989–5992; *Angew. Chem.* **2008**, *120*, 6078–6081.

[15] C. Wu, R. Li, D. Dearborn, Y. Wang, *Int J Org Chem* **2012**, *2*, 22.

[16] a) D. E. Clark, *Drug Discovery Today* **2003**, *8*, 927–933; b) V. W. Pike, *Trends Pharmacol. Sci.* **2009**, *30*, 431–440; c) S. A. Hitchcock, L. D. Pennington, *J. Med. Chem.* **2006**, *49*, 7559–7583.

[17] C. Vraka, L. Nics, K. H. Wagner, M. Hacker, W. Wadsak, M. Mitterhauser, *Nucl. Med. Biol.* **2017**, *50*, 1–10.